Bioresource Technology

Study on thermochemical characteristics properties and pyrolysis kinetics of the mixtures of waste corn stalk and pyrolusite
--Manuscript Draft--

Manuscript Number:	BITE-D-20-08108R4
Article Type:	Original research paper
Keywords:	pyrolusite; waste biomass; thermodynamic analysis; mixed pyrolysis kinetics; non-isothermal models
Corresponding Author:	jin chen kunming university of science and technology kunming, CHINA
First Author:	Jinjia Du
Order of Authors:	Jinjia Du
	Lei Gao
	Yong Yang
	Guo Chen
	Shenghui Guo
	Mamdouh Omran
	jin chen
	Roger Ruan
Abstract:	As an alternative energy source for fossil energy, use of biomass pyrolysis to reduce pyrolusite is of great significance for energy conservation, emission reduction and environmental protection. Kinetics and thermodynamics of reducing pyrolusite using biomass pyrolysis was studied using thermogravimetric analysis analysis. Five non-isothermal methods, Flynn-Wall-Ozawa, Kissinger-Akahira-Sunose, Distributed Activation Energy Model, Starink and Friedman, were employed to calculate the pyrolysis kinetics and thermodynamic parameters. The results showed that pyrolusite reduction by biomass pyrolysis can be divided into four stages: drying stage (30-175 °C), rapid pyrolysis reduction stage (175-350 °C), slow pyrolysis reduction stage (350-680 °C) and char formation stage (680-900 °C). The apparent activation energy, reaction enthalpy, Gibbs free energy and entropy change of pyrolusite reduction by biomass pyrolysis was calculated ranges from 170-180 kJ/mol, 164-174 kJ/mol, 136.97-137.25 kJ/mol and 45.67-61.91 J/mol·K, respectively. This work provides theoretical basis and practical guidance for the reduction of pyrolusite by waste corn stalk.

The main highlights of this work are as follows,

1. Process analysis of pyrolusite reduction by biomass pyrolysis is reported.

2. Thermodynamic analysis confirmed the pyrolusite reduction by biomass pyrolysis.

3. The kinetics and thermodynamics of reduction process were calculated.

Study on thermochemical characteristics properties and pyrolysis kinetics of the mixtures of waste corn stalk and pyrolusite

Jinjia Du [a], Lei Gao [b], Yong Yang [c], Guo Chen [a, b], Shenghui Guo [a], Mamdouh Omran [d],

Jin Chen [a, b, *], Roger Ruan [e]

a Faculty of Metallurgical and Energy Engineering, Kunming University of Science and

Technology, Kunming 650093, China.

b Key Laboratory of Green-Chemistry Materials in University of Yunnan Province, Yunnan

Minzu University, Kunming 650500, China.

c Daxin branch of CITIC Dameng Mining Industries Ltd., Chongzuo 532315, China.

d Faculty of Technology, University of Oulu, Finland.

e Center for Biorefining and Department of Bioproducts and Biosystems Engineering

University of Minnesota, 1390 Eckles Ave., St. Paul MN 55108, USA.

* Corresponding author: jinchen@kust.edu.cn

Abstract

As an alternative energy source for fossil energy, use of biomass pyrolysis to reduce pyrolusite is of great significance for energy conservation, emission reduction and environmental protection. Kinetics and thermodynamics of reducing pyrolusite using biomass pyrolysis was studied using thermogravimetric analysis analysis. Five non-isothermal methods, Flynn-Wall-Ozawa, Kissinger-Akahira-Sunose, Distributed Activation Energy Model, Starink and Friedman, were employed to calculate the pyrolysis kinetics and thermodynamic parameters. The results showed that pyrolusite reduction by biomass pyrolysis can be divided into four stages: drying stage (30-175 °C), rapid pyrolysis reduction stage (175-350 °C), slow pyrolysis reduction stage (350-680 °C) and char formation stage (680-900 °C). The apparent activation energy, reaction enthalpy, Gibbs free energy and entropy change of pyrolusite reduction by biomass pyrolysis was calculated ranges from 170-180 kJ/mol, 164-174 kJ/mol, 136.97-137.25 kJ/mol and 45.67-61.91 J/mol·K, respectively. This work provides theoretical basis and practical guidance for the reduction of pyrolusite by waste corn stalk.

Keywords: pyrolusite; waste biomass; thermodynamic analysis; mixed pyrolysis kinetics; non-isothermal models

1. **Introduction**

Energy is the most basic driving force for the development and economic growth of the whole world, and is the basis for human survival. Unfortunately, some of the world's conventional energy reserves can only last half a century (such as oil), the most can only

2

maintain a century or two (such as coal) of the needs of human survival (Guerrero et al., 2018; Jonasson et al., 2020; Mishra et al., 2020; Perez et al., 2018; Suganya, 2018). Therefore, it is urgent to develop clean and efficient conversion technology for alternative energy (Abnisa, 2014; Li et al., 2021). Biomass has attracted more and more attention because of its benefits in reducing the consumption of fossil energy and the impact of global warming (Jeswani et al., 2019; Rahpeyma & Raheb, 2019). It is a new resource that people pay close attention to in recent years, and biomass may play a relevant role in implementing sustainable routes that help to reduce carbon dioxide emissions. Biomass energy refers to a kind of precious renewable energy, which provides material resources with various abilities and powers for human production and life, and is an important material foundation of the national economy (Fillol et al., 2017). Biomass is mainly composed of cellulose, hemicellulose, and lignin (Jonasson et al., 2020; Liu et al., 2014; Lu, 2019; Stylianos D. Stefanidis, 2014).

Thermochemical conversion technologies include biomass gasification, dry distillation, and rapid pyrolysis liquefaction technologies. Biomass can be converted into solid products, liquid products and gas products with reductive properties, as well as harmless waste by thermochemical conversion technology. Therefore, from the perspective of environmental protection, biomass pyrolysis process and its subsequent metallurgical application is an ideal technology for the utilisation of biomass energy resources.

As an important industrial raw material, manganese is widely used in metallurgy, electronic batteries, light, chemical and other industries (Perez et al., 2018; Sun, 2018), At present, the main reduction method of manganese dioxide is carbothermic reduction roasting, which is relatively mature. However, it has high quality requirements for coal, and coal is a

3

non-renewable resource, which is not conducive to sustainable development. Tian et al. used high-quality coal as a reducing agent to reduce low-grade pyrolusite, and the reduction degree of pyrolusite was over 93% (Tian et al., 2009). Biomass coke and activated carbon powder as reducing agents were employed to reduction by Feng et al. Results shown biomass coke has a shorter reduction time and a reduction efficiency of 98% than activated carbon powder (Feng et al., 2015). Recently, many scholars have begun to study microwave as a heat source to reduce pyrolusite. Studies by Luo et al. have shown that adding 10% coal powder to pyrolusite, heating to 500 °C with microwave and reacting for 30 min. The reduction degree of pyrolusite was above 94%, which can realize the efficient leaching of manganese (Luo, 2012). Li et al. proposed a method for reducing low-grade pyrolusite by microwave pyrolysis of walnut shells (Li et al., 2019), which provided a new idea for the reduction of pyrolusite by biomass. Biomass, as a cheap and easily available renewable resource, is used to reduce low-grade pyrolusite, which is of great significance for energy conservation, emission reduction, energy consumption, and greenhouse effect reduction.

The pyrolysis process is carried out through a series of very complex competitive reactions and simultaneous reactions, so the exact mechanism of pyrolysis is still controversial. When studying the pyrolysis mechanism of biomass, considering the complexity of pyrolysis process, clear kinetic models with reasonable assumptions to describe the complex physical and chemical process under different working conditions were widely used. Different mathematical models have been established by scholars to study the pyrolysis characteristcs of biomass with thermogravimetric analysis technology, which is an effective and efficient method for studying the kinetics of biomass pyrolysis. Kissinger, distributed

4

activation energy and starink model have been widely employed to evaluate and explain the kinetics of the biomass pyrolysis because these models have several advantages, including simplicity and accuracy (Gao, 2018; Li, 2018; Patel et al., 2018). Currently, the two most important models for predicting the kinetics of biomass pyrolysis are the isothermal and the non-isothermal methods (Arshad, 2020). The non-isothermal model has a lower error range and requires less experimental data than isothermal model (Xu et al., 2020).

The pyrolysis kinetic parameters were calculated by many researchers with thermogravimetric analysis technology. For instance, Mishra et al. studied the kinetic characteristics and pyrolysis behavior of waste biomass imza (NM) and Phyllanthus emblica (AM) (Mishra et al., 2020). Lin et al. established a kinetic model of bagasse, sludge and their mixture applied by distribution activation energy model (DAEM) (Lin et al., 2019). The non-isothermal thermogravimetric method was applied to investigate the pyrolysis kinetics of nine kinds of poplar genotype. The activation energy values obtained by two of iso-conversional methods, namely Flynn-Wall-Ozawa (FWO) and Kissinger-Akahira-Sunose (KAS), were similar (Rego et al., 2020). Li et al. revealed the mechanism of low-temperature reduction of high-iron Bayer process red mud by pine sawdust using thermogravimetric and kinetic analysis (Li et al., 2017). However, there are few reports on the thermodynamics and kinetics of pyrolusite reduction by biomass pyrolysis. Hence, this work extends the knowledge into the pyrolysis reduction mechanism of multi-component in the mixture of biomass and pyrolusite.

In this study, the TG-DTG analysis method was used to analyze the co-pyrolysis reduction characteristics of waste straw and pyrolusite, and the kinetics and thermodynamics

5

of the process of pyrolusite reduction by biomass pyrolysis were studied. From the perspective of thermodynamics analysis, the possibility of pyrolusite reduction by biomass pyrolysis and the possible chemical reactions was confirmed. Five of iso-conversional methods, namely Friedman (FM), Kissinger-Akhira-Sunose (KAS), Flynn-Wall-Ozawa (FWO), Distributed activation energy model (DAEM) and Starink method s, were employed the co-pyrolysis reduction between waste straw and pyrolusite, aiming to study the thermodynamics and kinetics parameters. Based on the thermodynamics and kinetics analysis of pyrolusite reduction by biomass pyrolysis, important basic data were provided for the research and development of biomass thermochemical conversion technology and the reduction of pyrolusite.

2. Materials and methods

2.1. Materials

The pyrolusite (ω(Mn)=28.81%) used in the study was taken from Zhongxing manganese company, Guangxi Province, China. After drying (105 °C), crushing and grinding, the fine powder with the particle size of 120 to 200 meshes was obtained. The measured median diameter (D_{50}) of pyrolusite is 24.59 μm, as shown in Fig. 1.

The biomass used in the study were the waste corn stalk (D_{50}=141.46 μm), as shown in Fig. 1, received from Lian Yungang City, Jiangsu Province, China. The proximate analysis was performed with the National Standard of the People's Republic of China (GB/T28731-2012) and Solid Biofuel Technical Specification of EU (CEN/TC355), and the elemental content study was executed in an elemental analyzer provided by Advanced

6

Analysis and measurement Center of Yunnan University. The analytical results were shown in Table 1.

2.2. Characterization

The characteristic test of pyrolusite reduction by biomass pyrolysis was carried out on a simultaneous thermal analyzer (SAT 449F3, NETZSCH, Germany). During the test, pyrolusite and biomass were put into the alumina crucible in a certain proportion (Bio%=10, 20, 30, 40 and 50%), and high-purity nitrogen was introduced as protective gas (flow rate 100 mL/min). The heating rate was 10 °C/min, and the temperature range was 30 to 900 °C. At the same time, the reduction of pyrolusite by biomass pyrolysis was further studied at three different heating rates of 10, 20 and 40 °C/min. Fourier-transform infrared spectroscopy (IS, Nicolet, USA) with a spectral region of 4000-400 cm^{-1} was employed to analyzed the biomass material and the pyrolysis products. The low-grade pyrolusite and the reduction products were confirmed by X-ray diffractometer (D8 ADVANCE A25X, Bruker, Germany). The microstructures of the reduction products at different temperatures were analyzed by a field-emission scanning electron microscope (XL30ESEM-TM, Philips, Netherlands).

2.3. Thermodynamics analysis

The thermodynamic parameters, reaction enthalpy, entropy and Gibbs free energy formula are provided as follows,

$$-\frac{E}{RT} + \ln A = -\frac{\Delta G^{\neq}}{RT} + \ln \frac{k_B T}{h} \tag{1}$$

$$\Delta H^{\neq} = E - RT \tag{2}$$

$$\Delta G^{\neq} = \Delta H^{\neq} - T\Delta S^{\neq} \tag{3}$$

where A is the frequency factor, (min^{-1}), k_B is Boltzmann constant (1.38×10^{-23} J K^{-1}), and

7

h is Plank constant (6.626×10^{-34}).

2.4. Kinetic theory

Based on the thermodynamic analysis of the pyrolusite reduction of biomass pyrolysis, the possibility of the reaction can be expected, and its kinetic mechanism will be discussed further below.

The biomass pyrolysis reaction is generally regarded as a first-order reaction. The weight loss rate of biomass in the pyrolysis reaction can be expressed as:

$$\frac{d\alpha}{dt} = kf(\alpha) \tag{4}$$

$$\alpha = \frac{m_0 - m_t}{m_0 - m_f} \tag{5}$$

where α = conversion value, m_0, m_t and m_f are the initial mass, the mass at a specific time and the final mass, respectively, k = reaction rate constant. It was assumed that the transformation of biomass into targeted products occurred in the single-step process; then the reaction rate (k) can be inscribed as:

$$k = A\exp(-\frac{E}{RT}) \tag{6}$$

where E = activation energy, (kJ mol^{-1}), A = pre-exponential factor, (min^{-1}), R = Gas constant, (8.314 J mol^{-1} K^{-1}, T = Absolute temperature, (K).

Combining Eq. (1) and Eq. (3), the Eq. (4) can be obtained:

$$\frac{d\alpha}{dT} = \frac{d\alpha}{dt}\frac{dt}{dT} = \frac{A}{\beta}exp(-\frac{E}{RT})f(\alpha) \tag{7}$$

where β = the rate of heating. Separate the variables of Eq. (4) and integrate on both sides to obtain:

$$g(\alpha) = \int_0^\alpha \frac{d\alpha}{f(\alpha)} = \frac{A}{\beta}\int_{T_0}^T \exp(-\frac{E}{RT})\,dT \tag{8}$$

where $g(\alpha)$ = conversion integral.

8

2.4.1. Friedman method (FM)

Friedman (FM) model is the first and simplest iso-conversional model, the simplified FM model can be expressed as:

$$\ln\left(\frac{d\alpha}{dt}\right) = \ln[Af(\alpha)] - \frac{E_a}{RT} \tag{9}$$

The slope $-E_a/R$ can be calculated by the linear plot between $\ln(d\alpha/dt)$ against $1/T$.

2.4.2. Flynn-Wall-Ozawa (FWO)

Flynn-Wall-Ozawa (FWO), as an integral iso-conversional model, has been recognized as a more accurate estimation of activation energy. Under different heating rate β, the slope is $-1.052E_a/R$ can be calculated through the kinetic curve reflecting a linear relationship between $\ln\beta$ and $1/T_\alpha$. The simplified FWO model can be expressed as:

$$\ln\beta = -1.052\frac{E_a}{RT_\alpha} + \ln\left(\frac{AE_a}{RG(\alpha)}\right) - 5.331 \tag{10}$$

2.4.3. Kissinger-Akahira-Sunose (KAS)

The Kissinger-Akahira-Sunose model is the most widely used method for calculating kinetic parameters from non-isothermal thermogravimetric kinetic data. For the KAS model, the representative equation is Eq. (11). Under different heating rate β, the linear plot between $\ln(\beta/T_\alpha^2)$ versus $1/T_\alpha$ provided slope $-E_a/R$, So the activation energy and frequency factor can be obtained.

$$\ln\left(\frac{\beta}{T_\alpha^2}\right) = -\frac{E_a}{RT_\alpha} + \ln\left(\frac{AR}{E_a G(\alpha)}\right) \tag{11}$$

2.4.4. Distributed activation energy model (DAEM)

Distributed activation energy model (DAEM) is an effective method to deal with the reaction behavior of complex systems including infinite parallel first-order reactions, and is

9

often used to describe complex processes such as biomass pyrolysis. The simplified DAEM model can be expressed as:

$$\ln\left(\frac{\beta}{T_\alpha^2}\right) = -\frac{E_a}{RT_\alpha} + \ln\left(\frac{AR}{E_a}\right) + 0.6075 \tag{12}$$

2.4.5. Starink method

The Starink method was generally considered more accurate in the process of biomass pyrolysis. Therefore, the Starink method was empolyed to study the kinetics of the pyrolysis reduction process, and the simplified model can be written as:

$$\ln\left(\frac{\beta}{T_\alpha^{1.8}}\right) = C - 2.3111\frac{E_a}{RT_\alpha} \tag{13}$$

3. Results and discussion

3.1. Fourier transform infrared spectroscopy (FT-IR)

FT-IR analysis was conducted to verify the conversion of biomass pyrolysis in the pyrolysis process. It can be observed that after the biomass pyrolysis, the peak at 3403.21cm^{-1} is caused by the O-H stretching vibration, indicating the presence of alcohol or carboxylic acid compounds; The strong vibration peaks of C-H groups at 2958.39 and 1382.77 cm^{-1} confirmed the existence of alkanes, alkenes or aromatic hydrocarbons. The peaks at 1458.95 and 1382.77 cm^{-1} are due to bending vibration of Alkyl C-C bond, while the four peaks at 1247.72, 1220.58, 1101.68 and 1060.19 cm^{-1} are assigned to C-O stretching vibration indicated presence of ether, ester, alcohol and phenolic compounds. The characteristic stretching vibration peaks of benzene ring C=C bond at 1599.73 and 1515.84 cm^{-1}, and absorption peaks at 876.65, 834.28 and 754.06 cm^{-1} further indicate the existence of various aromatic compounds in the liquid tar product; The characteristic stretching vibration peaks

10

assigned to benzene ring C=C bond at 1599.73 and 1515.84 cm^{-1}, and absorption peaks at 876.65, 834.28 and 754.06 cm^{-1} further indicate the existence of various aromatic compounds in the liquid tar product; The appearance of strong absorption at 1716.14 cm^{-1} can be attributed to the C=O stretching vibration of the exsitence of aldehydes, ketones, acids or esters. The new characteristic peak at 748.17 cm^{-1} are designated to the O-H bending, demonstrating the existence of mono and polycyclic substituted aromatics compounds.

3.2. Thermo-dynamic calculation

Thermo-gravimetric analysis and thermo-dynamic calculation of the mixture of biomass and pyrolusite were carried out to deeply investigate whether the process of biomass pyrolysis and reduction of pyrolusite is feasible, and preliminarily study the mechanism of biomass pyrolytic reduction of pyrolusite. The mixture of biomass and pyrolusite (bio% = 40%) was analyzed by thermo-gravimetry at a heating rate of 10 °C/min, as shown in Fig. 2(a). Small molecular products mainly including reducing volatiles (carbon monoxide (CO), hydrogen (H$_2$), methane (CH$_4$)) and a small amount of biochar (C) were generated through biomass pyrolysis in the atmosphere of inert gas. Therefore, the reduction process of pyrolusite by carbon mon oxide (CO) and biochar (C) was studied, and the relationship between Gibbs free energy and temperature was calculated by Factsage 7.0, as shown in Fig. 2(b) and Fig. 2(c)

It can be seen from Fig. 2(a) that the process of low-grade pyrolysite reduction by biomass pyrolysis can be roughly divided into three stages, namely drying stage, activated pyrolysis reduction stage and carbon reduction stage. The temperature ranges of drying stage, activation pyrolysis reduction stage and carbon reduction stage were 30 to 175 °C, 175 to 650 °C and 650 to 900 °C, respectively. Free water, bound water and light hydrocarbon in

11

biomass and pyrolusite were removed in the drying stage. Thermogravimetric analysis

showed that the TGA curve of the mixture decreased significantly during the activation

pyrolysis reduction stage (175 to 650 °C). Ranjeet et al. confirmed the decomposition of

hemicellulose and cellulose at 180 to 300 °C and 300 to 480 °C (Mishra et al., 2020). Li et al.

confirmed that a large amount of volatile gas components (CO, CO_2, H_2, CH_4, etc.) and

biochar (C) were generated between 150 to 480 °C attributed to the pyrolysis of hemicellulose

and cellulose (Li et al., 2019). The results shown that at this stage, the gas-solid reaction

related to the quality change began to occur due to the interaction between the reducing

volatile gas produced by the pyrolysis of the biomass and the pyrolusite. According to Fig.

2(b), MnO_2 can be reduced to MnO by CO in the whole temperature range (30 to 900 °C).

Therefore, the main gas-solid reaction, i.e. $MnO_2 \rightarrow Mn_2O_3 \rightarrow Mn_3O_4 \rightarrow MnO$ reaction (Zhang,

2013a; Zhang, 2013b), can occur between 175 °C and 650 °C in the activation pyrolysis

reduction stage. In addition, a small amount of Fe_2O_3 can be reduced to Fe_3O_4 by CO.

According to Fig. 1(a) and Fig. 1(c), for solid-solid reaction, Mn_3O_4 and Fe_2O_3 begin to be

reduced by biochar (C) to produce MnO and Fe_3O_4, and the minimum temperatures were

284.0 °C and 322.6 °C, respectively. The TGA curve by Li et al. confirmed that the maximum

weight loss peak at 320 °C was caused by the reduction of Mn_3O_4 to MnO (Li et al., 2019).

Therefore, according to Fig. 2(a), it can be seen that around 340.5 °C, there was a drop in the

TGA curve and a peak in the DTG curve, which was mainly attributed to the reduction of

Mn_3O_4 and Fe_2O_3. Regardless of the reduction of pyrolusite by CO and C, the thermodynamic

Gibbs free energy diagram shown that compared with the reduction process

$((Fe_2O_3 \rightarrow Fe_3O_4 \rightarrow FeO))$, manganese oxide was more easily reduced by CO and C to

low-valent oxides. With the increase of temperature, the pyrolysis reduction reaction entered the carbon reduction stage (650 to 900 °C), in which a large amount of biochar (C) began to accumulate. The mechanism of pyrolysis reduction changed from gas-solid reaction to solid-solid reaction. The unreacted MnO_2, Mn_2O_3, Mn_3O_4 and Fe_2O_3 continued to take part in the carbon reduction reaction. In addition, the materials (MnO, Fe_3O_4 and FeO) that failed to participate in the reaction also began to react in the high-temperature region due to the increase of temperature. Fig. 2(b) shows that when the temperature was higher than 701.5 °C, CO was generated and continued to participate in the gas-solid reaction due to the reaction of biochar (C) with CO_2. Fig. 2(c) shows that when the temperature was higher than 681.7 °C and 720.4 °C, Fe_2O_3 was reduced by biochar (C) to form Fe_3O_4 and Fe_3O_4 was reduced to form elemental metal Fe. Combined with Fig. 2, considering the pressure caused by impurities in the subsequent leaching process, to ensure the effective recovery of manganese and avoid the production of FeO, it is recommended to set the pyrolysis reduction temperature between 175 °C and 682 °C. The thermodynamic Gibbs free energy diagram of the reduction of pyrolusite by biomass pyrolysis shows that this reduction reaction process can be carried out. According to the analysis of the thermogravimetric curve, the mechanism of the process of reducing pyrolusite by the biomass was initially obtained.

3.3. Thermo-gravimetric analysis

To further confirm that the process and mechanism of reducing pyrolusite by biomass pyrolysis, thermogravimetric analysis (TGA) on the mixture of waste corn stalk and pyrolusite in different proportions (bio%=10, 20, 30, 40 and 50%) were conducted. Fig. 3 shows the TGA-DTG curves of different proportions of ratios of biomass content (bio%=10,

13

20, 30, 40 and 50%). The weight loss rate of the system gradually changes with the increase of the biomass content, and the changing trend of the system was the same during the pyrolysis reduction process. The interval between the increase in biomass content from 40 to 50% and the 30 to 40% weight loss rate was significantly shortened due to the over production of biochar caused by 50% biomass content. Therefore, the most appropriate biomass percentage for reducing pyrolusite by biomass should be between 30% and 50%. According to the thermogravimetric curve of the mixture of waste corn stalks and pyrolusite (Fig. 3), the thermal weight loss process can be roughly divided into four stages, namely the drying stage, the fast pyrolysis reduction stage, the slow pyrolysis reduction stage and the carbonization stage and the temperature ranges of the four stages were 30 to 175 °C, 175 to 350 °C, 350 to 650 °C and 650 to 900 °C, respectively. The first stage (30 to 175 °C) was the drying stage, resulting in free water and bound water escape from the surface of biomass and pyrolusite and some depolymerization reactions and a slow glass transition phenomenon occurred. Glass transition refers to the transition between the high elastic state and the glass state. From the molecular structure, the glass transition is a relaxation phenomenon of the amorphous part of the polymer from the frozen state to the thawed state. When biomass undergoes glass transition, its physical and mechanical properties change drastically; The cell structure changed, and functional groups including free radicals, carboxyl groups, and peroxy hydroxyl appeared, and a small amount of hydrogen (H_2) was produced (Mehrabian et al., 2012), which the total mass loss was 4 to 6%; When the temperature was above 240 °C, the thermogravimetric process of pyrolusite reduction by biomass entered the fast pyrolysis reduction stage, and the weight loss rate of the mixtures in this stage was the largest. Di Blasi

14

et al. confirmed the decomposition of hemicellulose at 225 to 325 ° C (Di Blasi, 2008), and

Ranjeet Kumar Mishra et al. also proved that the peaks observed at 236 ° C and 293 °C

confirmed the decomposition of hemicellulose, because hemicellulose has a characteristic

decomposition in the lower temperature range (200 to 340 °C) (Mishra et al., 2020).

According to the current research on hemicellulose cleavage pathway, the cleavage of

hemicellulose was firstly broken by C1-O5 to obtain the straight-chain sugar structure (R)

with aldehyde group at one end. Then C-C cleavage and reforming reaction were carried out

to form reductive products (CO, H_2 and a small amount of acetic acid). Among them, MnO_2

was reduced to Mn_2O_3 ($MnO_2 \rightarrow Mn_2O_3$), part of Mn_2O_3 was reduced to Mn_3O_4

($Mn_2O_3 \rightarrow Mn_3O_4$) and Fe_2O_3 in pyrolusite was partly reduced to Fe_3O_4 by CO; The third stage

(350 to 680 °C): According to reports, cellulose and lignin decompose in the temperature

range of 325 to 375 °C and 417 to 607 °C, respectively. Biochar (mainly C) also began to

form at this stage and participated in solid-solid reduction, and Mn_3O_4 and Fe_2O_3 began to be

reduced to low-valent metal oxides; As the temperature rises, the pyrolysis reduction entered

the fourth stage (680 to 900 °C), the C-O and C-H bonds were further broken, and the volatile

matter remaining in the charcoal was discharged. As the deep volatile matter diffuses to the

outer layer, fixed carbon was finally formed. As shown in Fig. 3, it was shown as a small drop

in the TGA curve and a small peak in the DTG curve near 680 °C. At this stage, Mn_3O_4 was

mainly reduced to MnO, part of the unreduced Mn_2O_3 was continuously reduced to Mn_3O_4,

and the biochar formed by biomass pyrolysis further reduces Fe_3O_4 and CO_2 produced in the

closed system was reduced by C to form CO volatilization, resulting in quality loss, thus

showing a small peak on the DTG curve.

15

3.4. Effect of heating rates

Fig. 4 shows the TGA-DTG curves with a biomass percentage of 40% at different heating rates. Under non-isothermal conditions, the pyrolysis reduction characteristics of pyrolusite reduced by biomass at three different heating rates (10, 20, and 40 °C/min) were studied. As the heating rate increased from 10 to 40 °C min^{-1}, although the corresponding time for the sample to reach the final set temperature decreased, the heat transfer hysteresis effect became more obvious. Therefore, the TGA-DTG curves of the samples showed a trend of moving to the high temperature side, and the temperature T_{max} corresponding to the maximum weight loss peak of DTG increased from 340.5 to 345.3 °C, respectively. It can be seen from Fig. 2 that around 680 °C, Mn_3O_4 is reduced, and some unreduced Mn_2O_3 is continuously reduced to low-valent manganese compounds. The reduction of Fe_3O_4 was further enhanced by biochar formed from biomass pyrolysis and the CO produced in the closed system by C reduction, thus showing a small peak on the DTG curve. The temperature T_{max} corresponding to the weight loss peak of DTG lags from 668.4 to 708.2 °C, respectively. The heating rate of 10 °C/min can make the heat stay in the mixture of biomass and pyrolusite for a long time compared to 40 °C/min, which is beneficial to the pyrolysis of biomass and the reduction of pyrolusite. At a higher heating rate, the volatile substances generated by biomass pyrolysis are discharged with nitrogen before participating in the reaction, and the time for the interaction between the pyrolusite and the biomass is reduced, so the residual mass is reduced. In addition, the peak values of the DTG curves under the three different heating rates were also quite different. The maximum weight loss rate of biomass reduction of pyrolusite increased from 7.92 to 14.46 %/min. Therefore, the mixed powder of biomass and pyrolusite contributes

16

to the reduction of pyrolusite at a lower heating rate.

3.5. Kinetic and thermodynamic analysis

Based on five non-isothermal models, namely FWO, KAS, DAEM, Starink and FM, the kinetics and thermodynamics of the mixtures under different heating rates were analyzed. It must be mentioned that most studies on the mechanism of biomass pyrolysis were based on the calculation of apparent activation energy E_a and pre-exponential factor A. Hence, further solving its thermodynamic parameters, activation enthalpy, Gibbs free energy, and activation entropy, can help us to reveal the mechanism of the pyrolusite reduction by biomass pyrolysis. The kinetic and thermodynamic parameters of activated pyrolysis reduction stage were calculated by FWO, KAS, DAEM, Starink and FM methods. The results were shown in Table 2 and Fig. 5.

As shown in Table 2, the apparent activation energy E_a and the pre-exponential factor A were calculated using FWO, KAS, DAEM, Starink and FM methods to perform linear regression fitting, and it was observed that the average apparent activation energy were 180. 04, 180.33, 170.58, 179.70 and 209.25 kJ/mol, respectively. And the average pre-exponential factors were 5.62E+16, 5.95E+16, 8.41E+15, 5.25E+16 and 4.24E+16 s^{-1}, respectively. Notably, the average apparent activation energy calculated using FWO, KAS and Starink methods was about 180 kJ/mol, while the values calculated by the FM method was 209.25 kJ/mol. In addition, it is significantly obvious from Fig. 5(b) that the pre-exponential factor A calculated by FM method was three orders of magnitude larger than the other four methods. Taking results calculated by FM method into account, we conclude that the average activation energy of pyrolytic reduction of pyrolusite is 170.58 to 180.33 kJ/mol. It can be seen from

17

Table 2 that the average fitting coefficients (R^2>0.91) of the FWO, KAS, DAEM and Starink

methods were all very high, indicating that the selected model conforms to the pyrolysis

reduction process. It can be seen from Fig. 5(a) that the apparent activation energy of

pyrolusite reduction by biomass fluctuates with the conversion rate, indicating that there are

complex multi-step reactions, including parallel reaction, competitive reaction and continuous

reaction. When the conversion value was less than 0.3, the apparent activation energy

increases as the conversion value increases, resulting from the pyrolysis reaction of

hemicellulose. The conversion value was between 0.3 and 0.6, the apparent activation energy

(E_a) fluctuated slightly, indicating that cellulose became the main component of pyrolytic

reduction of pyrolusite. Once the conversion value was greater than 0.6, lignin has reached

the temperature conditions for pyrolysis, resulting in lower apparent activation energy.

Interestingly, the apparent reaction activation energy diagram (Fig. 5(a)), the reaction

enthalpy diagram (Fig. 5(c)), and the Gibbs free energy diagram (Fig. 5(d)) show the same

trend, however, the entropy change diagram (Fig. 5(e)) is inverted. It can be seen from Table 2

that the Gibbs free energy of the five non-isothermal models is greater than zero ($\Delta G^{\neq}>0$),

indicating that the process of reducing pyrolusite by biomass pyrolysis is not spontaneous, but

requires external energy to be thermally decomposed. The average Gibbs free energy

calculated according to FWO, KAS, DAEM, Starink and FM models were 136.98, 136.97,

137.25, 136.99 and 137.02 kJ/mol, respectively. The average Gibbs free energy obtained by

these five methods has little change, and the Gibbs free energy is between 136.97 kJ/mol and

137.25 kJ/mol, showing that the Gibbs free energy calculated by these five methods is

accurate and reliable. The average activation enthalpies of FWO, KAS, DAEM, Starink and

18

FM models were 174.94, 175.72, 176.10, 165.85 and 199.01 kJ/mol, respectively. resulting that the pyrolusite reduction by biomass pyrolysis is an endothermic reaction under an inert gas nitrogen environment. Activation entropy refers to the microscopic changes in the material structure during the activation process to a certain extent. A negative value of entropy indicates that the degree of disorder of the bond dissociation product is lower than that of the reactant, while a positive value is the opposite. As a measure of system chaos, the larger the value, the more disorderly of the system, but the less orderly. From Table 2, the average activation entropies of FWO, KAS, DAEM, Starink and FM were 61.43 J/mol·K, 61.91 J/mol·K, 45.67J/mol·K, 60.87 J/mol·K and 59.07 J/mol·K, respectively.

3.6. Phase composition analysis

The crystal structure of pyrolusite reduction by corn stalk at different temperatures was characterized by XRD, and the reduction degree of pyrolusite at differents temperatures for 30min were studies when the mass ratio of biomass was 30%. The XRD pattern results indicate that the intermediate products of MnO_2 in the pyrolusite reduction by biomass were Mn_2O_3 and Mn_3O_4, and the products were MnO. From these pyrolysis reduction experiments, the four progressive reduction stages of MnO_2 can be clearly perceived as $MnO_2 \rightarrow Mn_2O_3 \rightarrow Mn_3O_4 \rightarrow MnO$. As can be seen from Fig. 7(b), the reduction temperature has significant influence on the reduction degree of the pyrolusite. At 600 °C, the reduction degree of pyrolusite reached 93.2%. Therefore, corn stover can be applied as an ideal reducing agent to replace traditional coal to reduce pyrolusite.

3.7. Microstruction characterization

High-resolution scanning electron microscope (SEM) images were employed to study

the microstructure of pyrolusite at different reduction temperatures. It can be seen that cracks of different sizes appear on the surface of low-grade pyrolusite at different temperatures, indicating that temperature has a significant effect on the reduction of low-grade pyrolusite. No cracks were observed on the surface of the low-grade pyrolusite at 300 °C, indicating that the MnO_2 on the surface of the pyrolusite was reduced by the biomass. At 400 °C, it can be observed that the small cracks on the surface began to form, indicating reducing gas can pass through these pores to further reduce Mn_2O_3, Mn_3O_4 and MnO_2 to MnO. Above 500 °C, it can be noticed that the cracks on the surface of the particles were obviously wide and deep, and the pyrolusite particles were gradually disintegrated attributed to diffusion of volatile gases generated by the biomass pyrolysis.

4. Conclusions

Based on the thermodynamic diagram of pyrolusite reduction by waste corn stalk, the pressure of subsequent leaching and impurity removal process was analyzed and comprehensively considered to ensure the effective recovery of manganese and avoid the generation of FeO. Therefore, the experimental temperature of pyrolusite reduction by biomass pyrolysis was set between 175 °C and 682 °C. FWO, KAS, DAEM, Starink and FM methods were used to calculate the thermodynamic and kinetic parameters. On the basis of these results we concluded that the apparent activation energy, reaction enthalpy, Gibbs free energy and entropy change of pyrolusite reduction by biomass pyrolysis.

20

CRediT authorship contribution statement

Jinjia Du: Conceptualization, Investigation, Writing-original draft. **Lei Gao**: Conceptualization, Investigation, Writing-original draft. **Yong Yang**: Writing-review & editing. **Guo Chen**: Writing-review & editing. **Shenghui Guo**: Supervision, Project administration, Writing-review & editing. **Mamdouh Omran**: Writing review & editing. **Jin Chen**: Funding acquisition, Writing-review & editing. **Roger Ruan**: Writing review & editing.

Declaration of Competing Interest

The authors declare that they have no known competing financial interests or personal relationships that could have appeared to influence the work reported in this paper

Appendix A. Supplementary data

E-supplementary data for this work can be found in e-version of this paper online.

References

1. Abnisa, F. 2014. A review on co-pyrolysis of biomass: An optional technique to obtain a

high-grade pyrolysis oil. *Energy Convers. Manage*, **87**, 71-85.

2. Arshad, M.A. 2020. Thermo-oxidative decomposition of multi-walled carbon nanotubes: Kinetics and thermodynamics. *Fullerenes Nanotubes and Carbon Nanostructures*, **28**(11), 857-868.

3. Di Blasi, C. 2008. Modeling chemical and physical processes of wood and biomass pyrolysis. *Prog. Energy Combust. Sci.*, **34**, 47-90.

4. Feng, Y.L., Zhang, S.Y., Li, H.R. 2015. Roasting Reduction and Its Kinetics of Low-Grade Pyrolusite by Biomass Char. *Journal of Northeastern University*, **36**(10), 1482-1486.

5. Fillol, E., Albarelo, T., Primerose, A., Wald, L., Linguet, L. 2017. Spatiotemporal indicators of solar energy potential in the Guiana Shield using GOES images. *Renewable Energy*, **111**, 11-25.

6. Gao, R., Liu, Ya., Xu, Zhenming. 2018. Synthesis of oil-based resin using pyrolysis oil produced by debromination pyrolysis of waste printed circuit boards. *Journal of Cleaner Production*, **203**, 645-654.

7. Guerrero, P., Gerardo, D.J., Pillai, V., Raj, A., Brito, J.L. 2018. Effects of fuel-bound methyl groups and fuel flow rate in the diffusion flames of aromatic fuels on the formation of volatile PAHs. *Combustion and Flame*, **198**, 412-427.

8. Jeswani, H.K., Whiting, A., Azapagic, A. 2019. Environmental and Economic Sustainability of Biomass Heat in the UK. *Energy Technology*, **8**(11).

9. Jonasson, S., Bunder, A., Niittyla, T., Oksman, K. 2020. Isolation and characterization of cellulose nanofibers from aspen wood using derivatizing and non-derivatizing pretreatments. *Cellulose*, **27**(1), 185-203.

22

10. Li, H., Liu, X.M., Chen, J.L. 2017. Medium-low temperature reduction of high-iron Bayer process red mud using biomass pine sawdust. *Chinese Journal of Engineering*, **39**(9), 1331-1338.

11. Li, K., Jiang, Q., Chen, G., Gao, L., Peng, J., Chen, Q., Koppala, S., Omran, M., Chen, J. 2021. Kinetics characteristics and microwave reduction behavior of walnut shell-pyrolusite blends. *Bioresour Technol*, **319**, 124172.

12. Li, K.Q., Chen, J., Chen, G., Peng, J.H., Ruan, R., Srinivasakannan, C. 2019. Microwave dielectric properties and thermochemical characteristics of the mixtures of walnut shell and manganese ore. *Bioresour Technol*, **286**, 121381.

13. Li, L., Wei, L.L., Liu, Y.G., Li, C.H., Ding, Y.M., Lu, S.X. 2018. Pyrolysis characteristic study on seat hard materials of China's high-speed train. *Journal of Thermal Analysis and Calorimetry*, **134**(3), 2107-2113.

14. Lin, Y., Tian, Y., Xia, Y., Fang, S., Liao, Y., Yu, Z., Ma, X. 2019. General distributed activation energy model (G-DAEM) on co-pyrolysis kinetics of bagasse and sewage sludge. *Bioresour Technol*, **273**, 545-555.

15. Liu, Y., Xu, Y., Zhang, F., Yun, J., Shen, Z. 2014. The impact of biofuel plantation on biodiversity: a review. *Science Bulletin*, **59**(34), 4639-4651.

16. Lu, X.Q., Li, C., Zhang, S.K., Wang, X.H., Zhang, W.Q., Wang, S.G., Xia, T. 2019. Enzymatic sugar production from elephant grass and reed straw through pretreatments and hydrolysis with addition of thioredoxin-His-S. *Biotechnology for Biofuels*, **12**(1), 297

17. Luo, S.Q. 2012. Research on Microwave heating process of deoxygenate restoring

23

pyrolusite. *Popular Science and Technology*, **1**, 62-64.

18. Mehrabian, R., Scharler, R., Obernberger, I. 2012. Effects of pyrolysis conditions on the heating rate in biomass particles and applicability of TGA kinetic parameters in particle thermal conversion modelling. *Fuel*, **93**, 567–575.

19. Mishra, R.K., Mohanty, K., Halder, P.K. 2020. Kinetic analysis and pyrolysis behaviour of waste biomass towards its bioenergy potential. *Bioresour Technol*, **311**, 123480.

20. Patel, S.R., Kundu, S.K., Halder, P.K., Setiawan, A., Paz-Ferreiro, J, Surapaneni, A., Shah, K.V. 2018. A Hybrid Kinetic Analysis of the Biosolids Pyrolysis using Thermogravimetric Analyser. *Chemistry select*, **3**(47), 13400-13407.

21. Perez, G.R., Bello, T.S., Rojas, M. 2018. Thermodynamic simulation of the reaction mechanism of Mn2+ oxidation with an SO2/O-2 mixture. *Hydrometallurgy*, **176**, 260-265.

22. Rahpeyma, S.S., Raheb, J. 2019. Microalgae Biodiesel as a Valuable Alternative to Fossil Fuels. *Bioenergy Research*, **12**(4), 958-965.

23. Rego, F., Soares, D., Casquilho, M., Fátami, C,R., Rodrigues, A. 2020. Pyrolysis Kinetics of Short Rotation Coppice Poplar Biomass. *Energy*. **207**(15), 118191.

24. Stylianos, D.S., Konstantinos, G.K., Eleni, F.I., Chrysoula, M.M., Petros, A. P., Angelos, A.L. 2014. A study of lignocellulosic biomass pyrolysis via the pyrolysis of cellulose, hemicellulose and lignin. *Journal of Analytical and Applied Pyrolysis*, **105**, 143-150.

25. Suganya, S., Kumar, P.S. 2018. Evaluation of environmental aspects of brew waste-based carbon production and its disposal scenario. *Journal of Cleaner Production*, **202**, 244-252.

24

26. Sun, B., Fazeli, F., Scott, C., Guo, B.Q., Aranas, C., Chu, X., Jahazi, M., Yue, S. 2018. Microstructural characteristics and tensile behavior of medium manganese steels with different manganese additions. *Mater. Sci. Eng*, **729**, 496-507.

27. Tian, Z.P., You, X.J., Peng, S.L. 2009. Application of High Efficiemcy MnO_2 by Reducing Furnace. *CHINA'S MANGANESE INDUSTRY*, **27**(2), 24-26.

28. Xu, S., Cao, B., Uzoejinwa, B.B., Odey, E.A., Wang, S., Shang, H., Li, C., Hu, Y., Wang, Q., Nwakaire, J.N. 2020. Synergistic effects of catalytic co-pyrolysis of macroalgae with waste plastics. *Process Safety and Environmental Protection*, **137**, 34-48.

29. Zhang, H.L., Zhu, G.C., Yan, H. Li, T.C., Zhao, Y.N. 2013a. The Mechanism on Biomass Reduction of Low-Grade Manganese Dioxide Ore. *Metallurgical and Materials Transactions B-Process Metallurgy and Materials Processing Science*, **44**(4), 889-896.

30. Zhang, H.L., Zhu, G.C., Yan, H., Zhao, Y.N., Li, T.C., Feng, X.J. 2013b. Reduction of Low-grade Manganese Dioxide Ore Pellets by Biomass Wheat Stalk. *Acta Metallurgica Sinica-English Letters*, **26**(2), 167-172.

Table 1 Main ultimate analysis and proximate analysis results of waste corn stalk powder (%).

Table 2 Kinetic and thermodynamic parameters calculation of FWO, KAS, DAEM, Starink and FM models.

Fig. 1. Particle size distributions of pyrolusite and corn stover powder.

Fig. 2. TG-DTG analysis of a mixture of 40% biomass and pyrolusite at 10 °C min^{-1} heating rate (a) and ΔG^{θ}-T diagram of pyrolusite reduced by biomass pyrolysis. (b) Carbon monoxide reduction reaction; (c) Carbon reduction reaction.

Fig. 3. Thermo-gravimetric analysis curve of mixed ratio of waste corn stalk and pyrolusite. (a) TGA curves; (b) DTG curves.

Fig. 4. Thermo-gravimetric analysis curve of different heating rate under mixed powder with biomass percentage of 40 %. (a) TG curves; (b) DTG curves.

Fig. 5. Kinetic and thermodynamic parameters with respect to conversion value. (a) average apparent activation energy (E_a); (b) average Pre-exponential factor (A); (c) average enthalpy of reaction ($\Delta H^{\neq}$); (d) average Gibbs free energy ($\Delta G^{\neq}$); (e) average entropy change ($\Delta S^{\neq}$).

27

Table 1 Main ultimate analysis and proximate analysis results of waste corn stalk powder (%).

Ultimate analysis					Proximate analysis			
C_{ad}	H_{ad}	O_{ad}	N_{ad}	S_{ad}	Moisture	Volatiles	Fixed carbon	Ash
45.22	6.05	40.62	1.06	0.16	13.92	62.95	19.20	3.93

Table 2 Kinetic and thermodynamic parameters calculation of FWO, KAS, DAEM, Starink and FM models.

Model	Conversion	E_a (kJ mol^{-1})	A (s^{-1})	$\Delta H^{\neq}$ (kJ mol^{-1})	$\Delta G^{\neq}$ (kJ mol^{-1})	$\Delta S^{\neq}$ (J mol^{-1}K^{-1})	R^2
FWO	0.1	127.99	1.59E+12	122.89	138.73	-25.63	0.9908
	0.2	138.19	1.25E+13	133.09	138.33	-8.48	0.9908
	0.3	193.34	8.03E+17	188.24	136.61	83.54	0.9727
	0.4	200.17	3.14E+18	195.07	136.43	94.89	0.9905
	0.5	209.74	2.12E+19	204.64	136.19	110.76	0.9325
	0.6	196.66	1.56E+18	191.56	136.52	87.38	0.9963
	0.7	199.56	2.78E+18	194.46	136.45	93.87	0.9906
	0.8	174.71	1.93E+16	169.61	137.13	52.56	0.8694
	Average	180.04	5.62E+16	174.94	136.98	61.43	0.9667
KAS	0.1	125.29	9.21E+11	120.19	138.84	-30.18	0.9894
	0.2	135.65	7.49E+12	130.55	138.43	-12.75	0.9894
	0.3	193.40	8.13E+17	188.30	136.61	83.64	0.7925
	0.4	193.97	9.11E+17	188.87	136.59	84.42	0.9894
	0.5	210.22	2.33E+19	205.12	136.18	111.55	0.9195
	0.6	215.80	7.09E+20	210.70	136.04	121.10	0.9951
	0.7	198.24	2.14E+18	193.14	136.48	91.68	0.9894
	0.8	170.06	7.61E+15	164.96	137.27	44.81	0.8489
	Average	180.33	5.95E+16	175.23	136.97	61.91	0.9392

	0.1	133.29	4.65E+12	128.19	138.52	-22.28	0.9894
	0.2	132.65	4.09E+12	127.55	138.55	-22.65	0.9894
	0.3	190.40	4.46E+17	185.30	136.69	73.74	0.7925
	0.4	180.97	6.77E+16	175.87	136.95	58.33	0.9894
DAEM	0.5	192.22	6.42E+17	187.12	136.64	77.38	0.9195
	0.6	185.80	1.78E+17	180.70	136.81	67.51	0.9951
	0.7	190.24	4.32E+17	185.14	136.69	73.69	0.9894
	0.8	159.06	8.37E+14	153.96	137.61	21.96	0.8489
	Average	170.58	8.41E+15	165.48	137.25	45.67	0.9392
	0.1	124.62	8.04E+11	119.52	138.87	-38.16	0.9895
	0.2	136.62	9.11E+12	131.52	138.39	-11.12	0.9895
	0.3	194.39	9.91E+17	189.29	136.58	85.29	0.7945
	0.4	190.98	5.01E+17	185.88	136.67	79.63	0.9895
Starink	0.5	211.27	2.88E+19	206.17	136.15	113.30	0.7950
	0.6	208.87	1.78E+19	203.77	136.21	109.32	0.9280
	0.7	199.41	2.70E+18	194.31	136.45	93.62	0.9895
	0.8	171.44	1.01E+16	166.34	137.23	47.10	0.8512
	Average	179.70	5.25E+16	174.60	136.99	60.87	0.9158
	0.1	133.33	4.69E+12	128.23	138.52	-16.65	0.9982
	0.2	166.39	3.64E+15	161.26	137.38	38.69	0.9889
FM	0.3	235.81	3.81E+21	230.71	135.59	153.92	0.9272
	0.4	237.37	5.19E+21	232.27	135.56	155.76	0.9299

0.5	240.59	9.85E+21	235.80	135.49	161.83	0.9680
0.6	249.90	6.27E+22	244.80	135.29	177.20	0.9664
0.7	249.92	6.29E+22	244.82	135.29	177.23	0.8564
0.8	165.58	3.10E+15	160.48	137.41	35.92	0.9453
Average	209.25	4.24E+16	173.52	137.02	59.07	0.9475
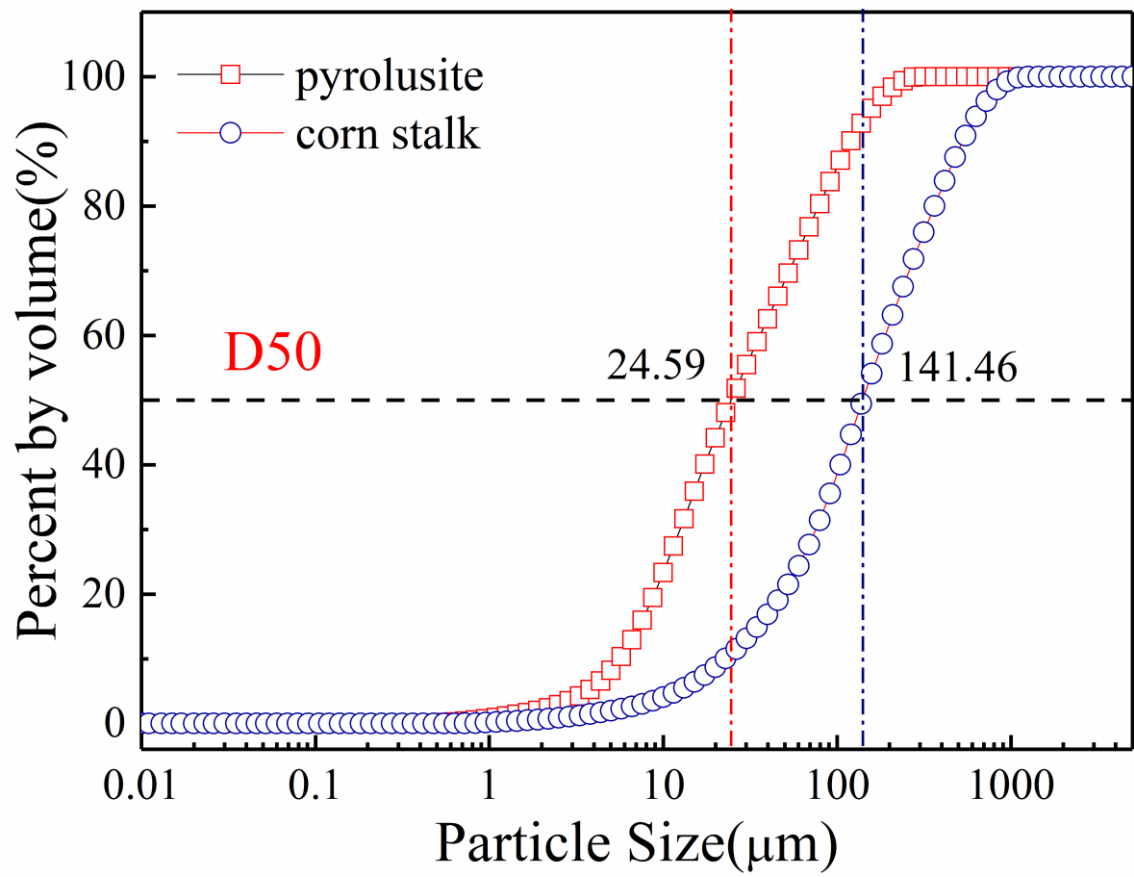
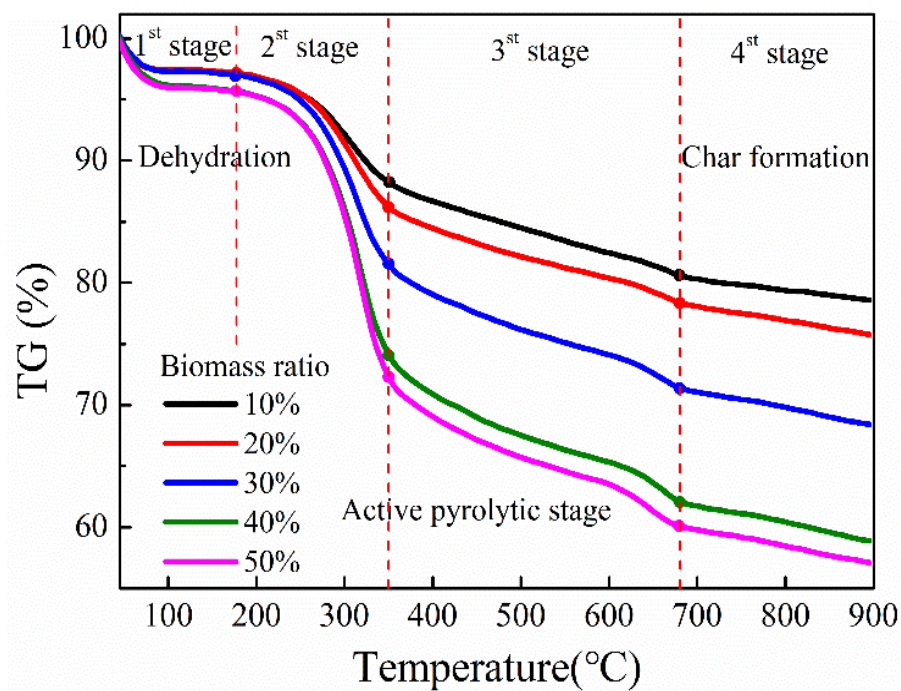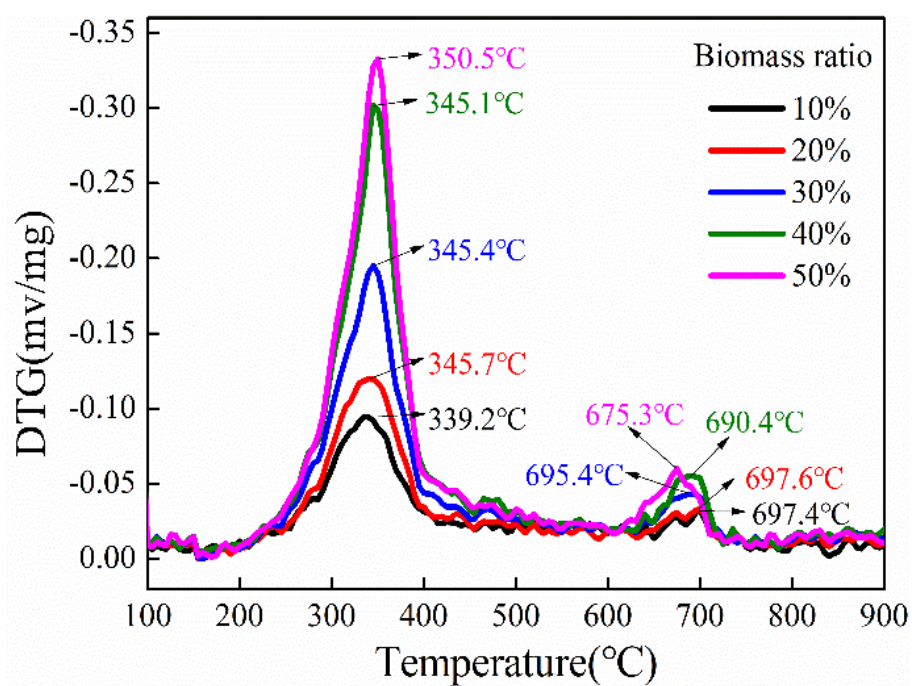Fig. 1. Particle size distributions of pyrolusite and corn stalk powder.
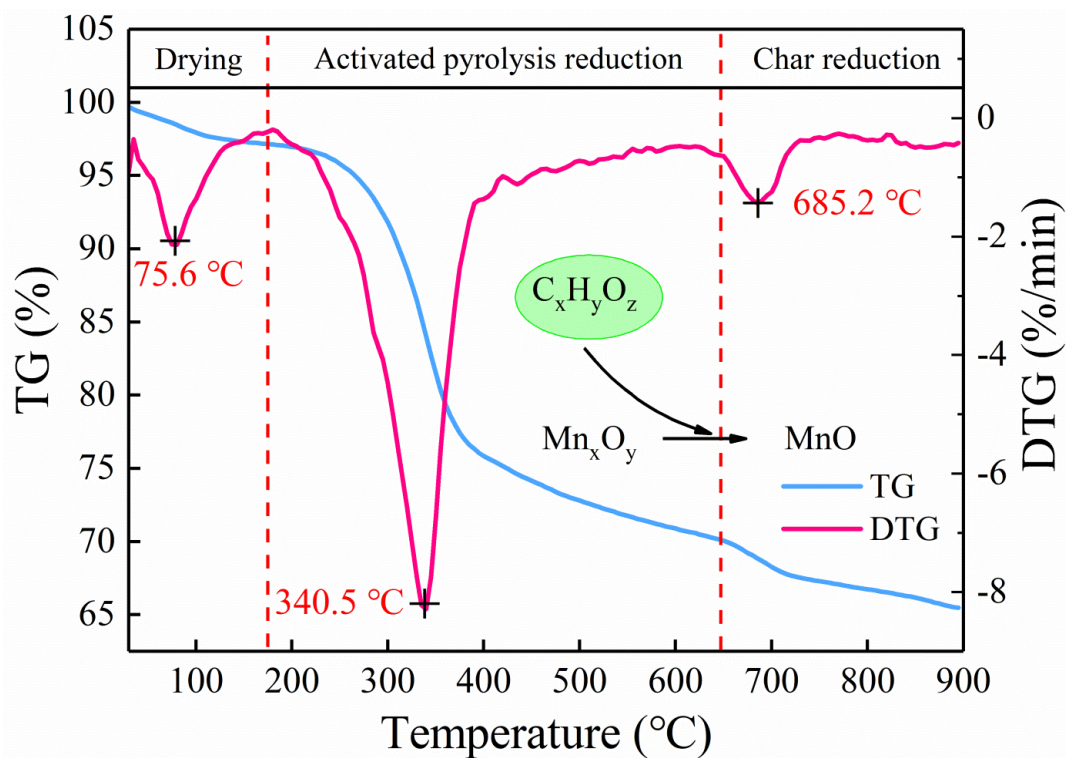
(a)
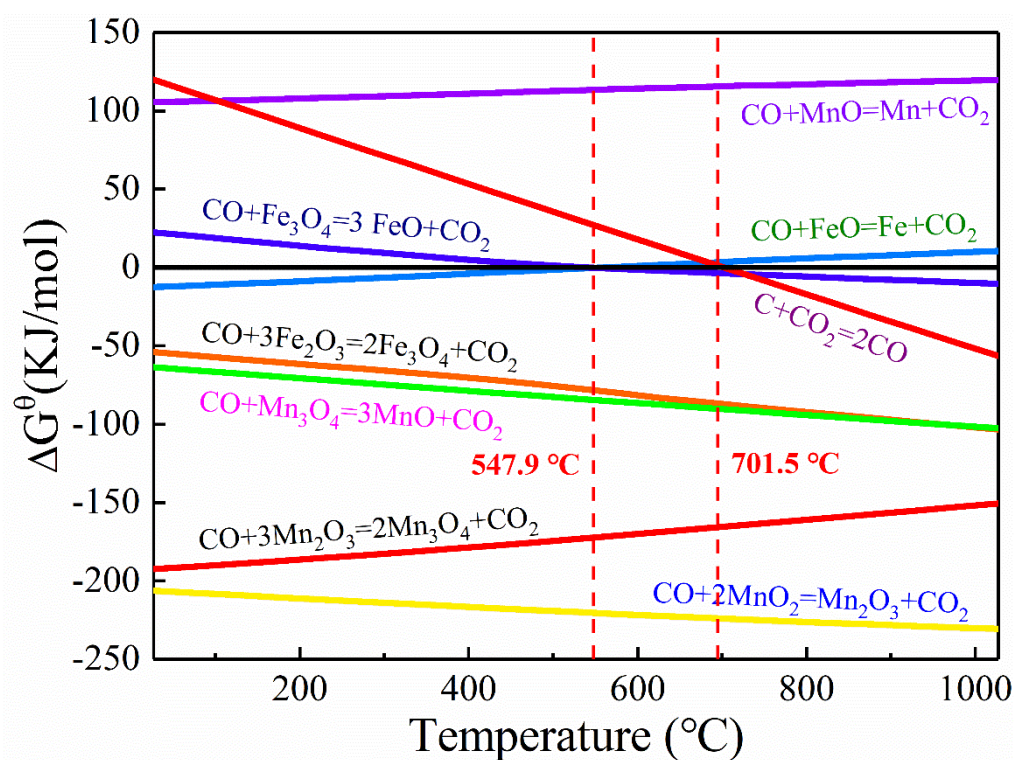
(b)
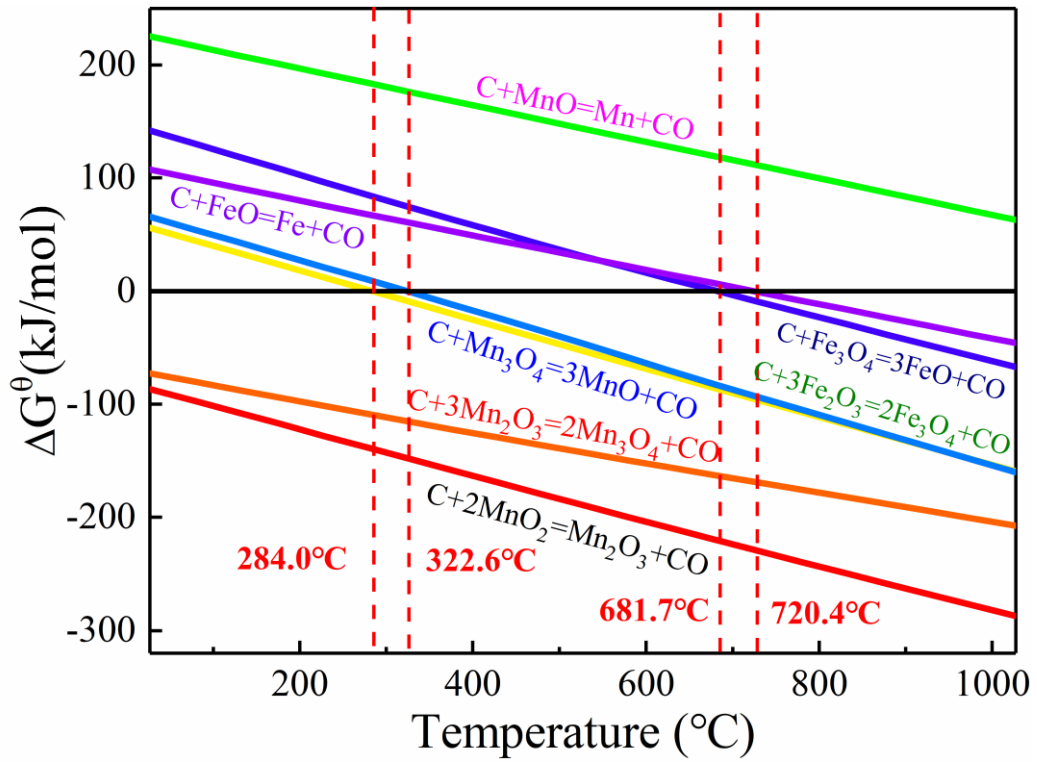
(c)

Fig. 2. TG-DTG analysis of a mixture of 40% biomass and pyrolusite at 10 °C min^{-1} heating rate (a) and ΔG^{θ}-T diagram of pyrolusite reduced by biomass pyrolysis. (b) Carbon monoxide reduction reaction; (c) Carbon reduction reaction.

(a)

(b)

Fig. 3. Thermo-gravimetric analysis curve of mixed ratio of waste corn stalk and pyrolusite. (a)

TGA curves; (b) DTG curves.
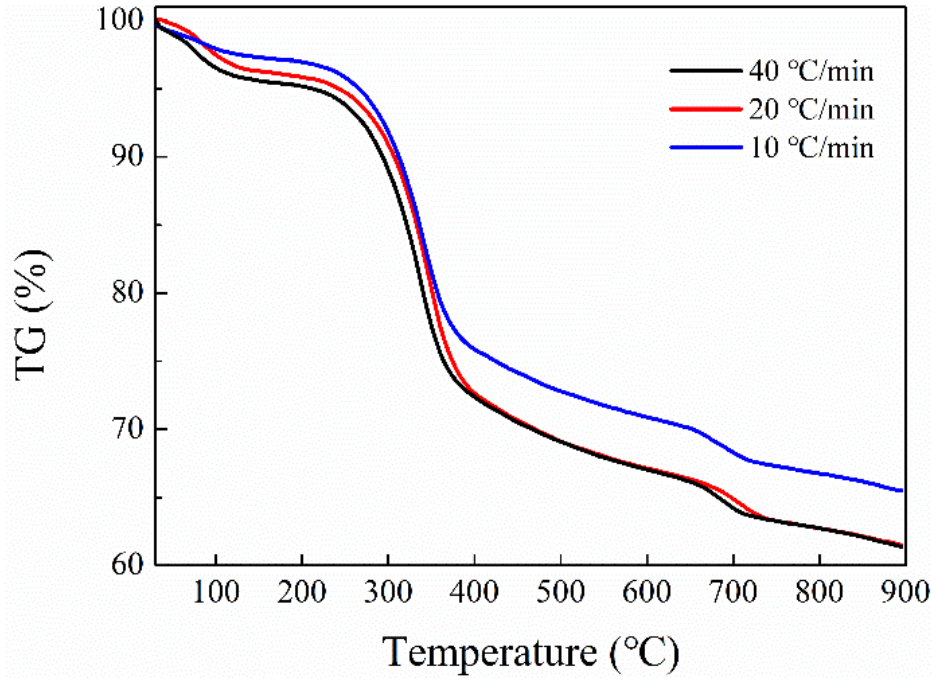
(a)
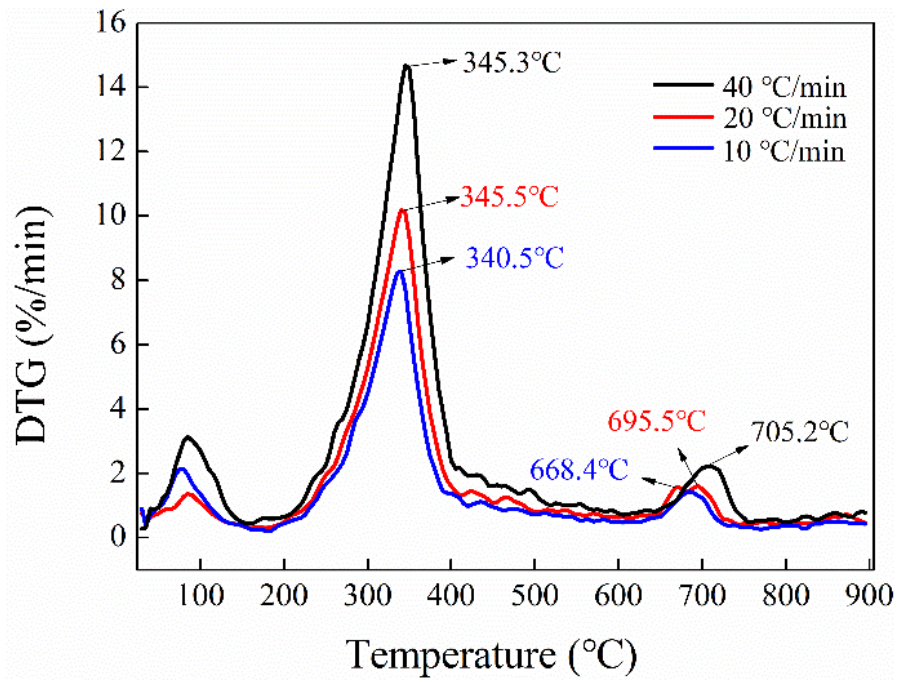
(b)

Fig. 4. Thermo-gravimetric analysis curve of different heating rate under mixed powder with

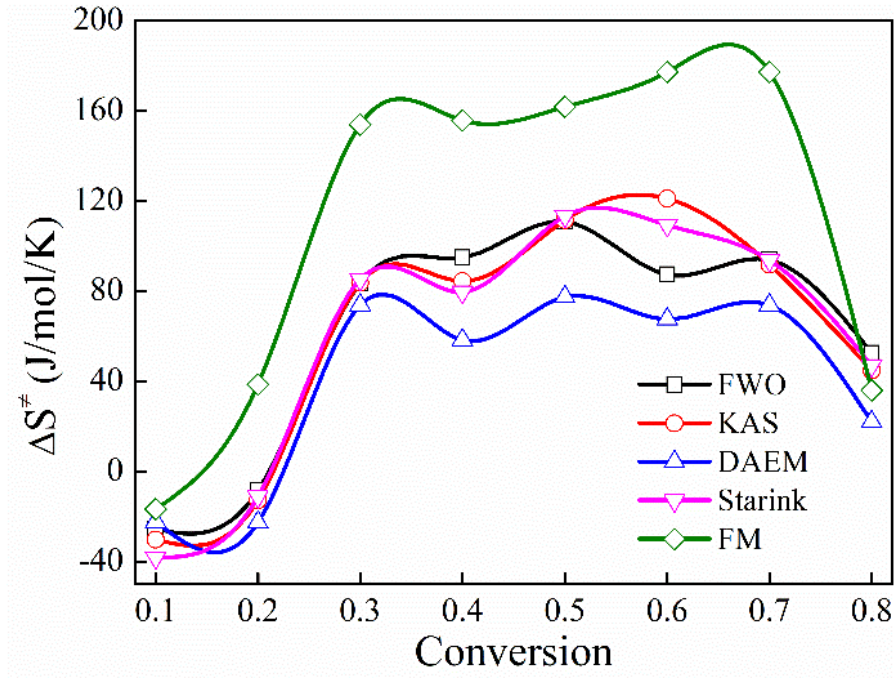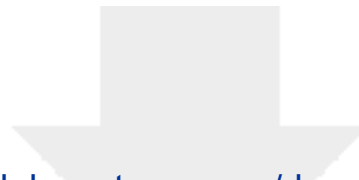biomass percentage of 40 %. (a) TG curves; (b) DTG curves.

(a)

(b)

37

(c)

(d)

38
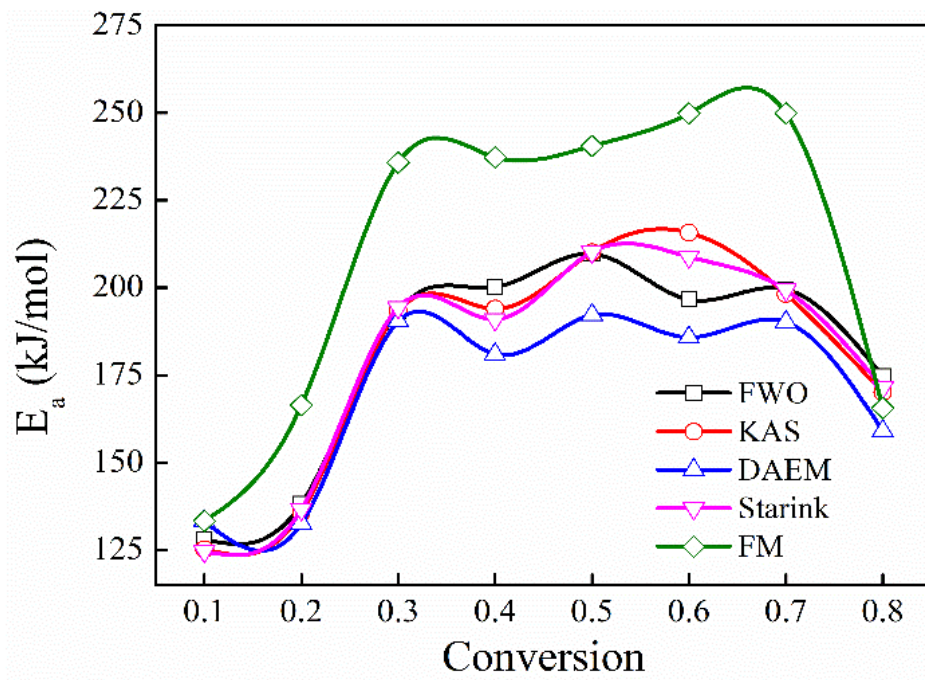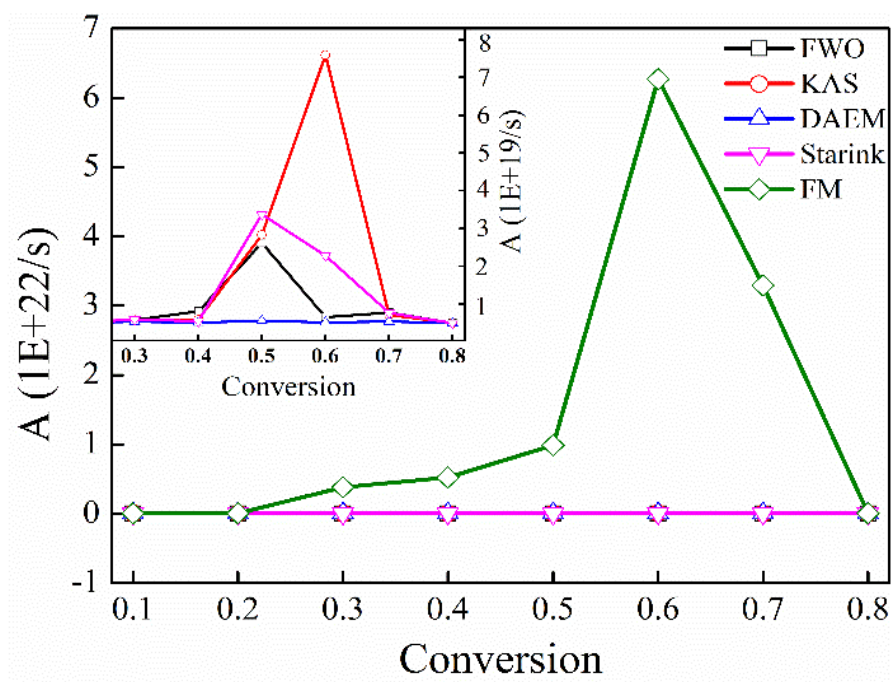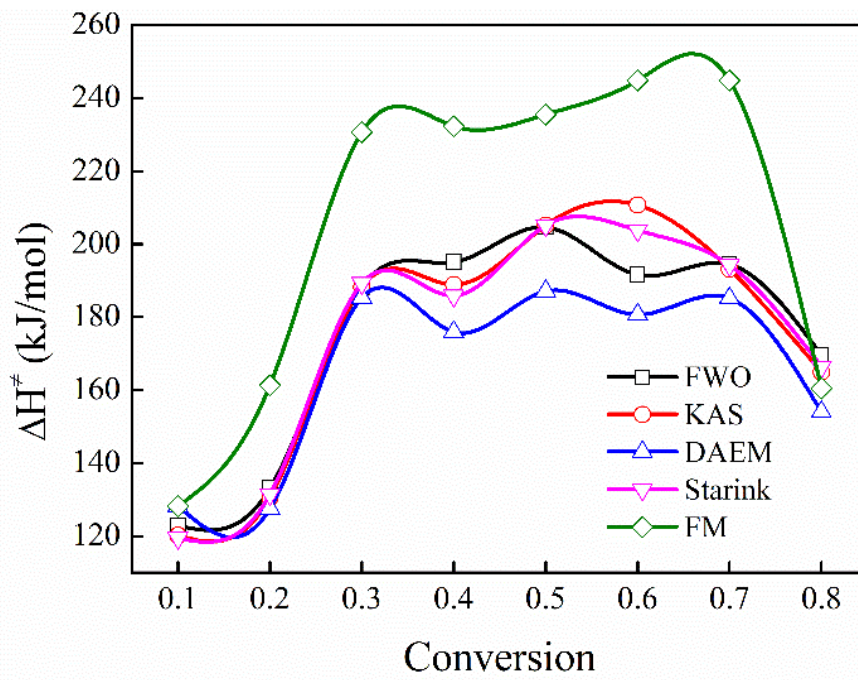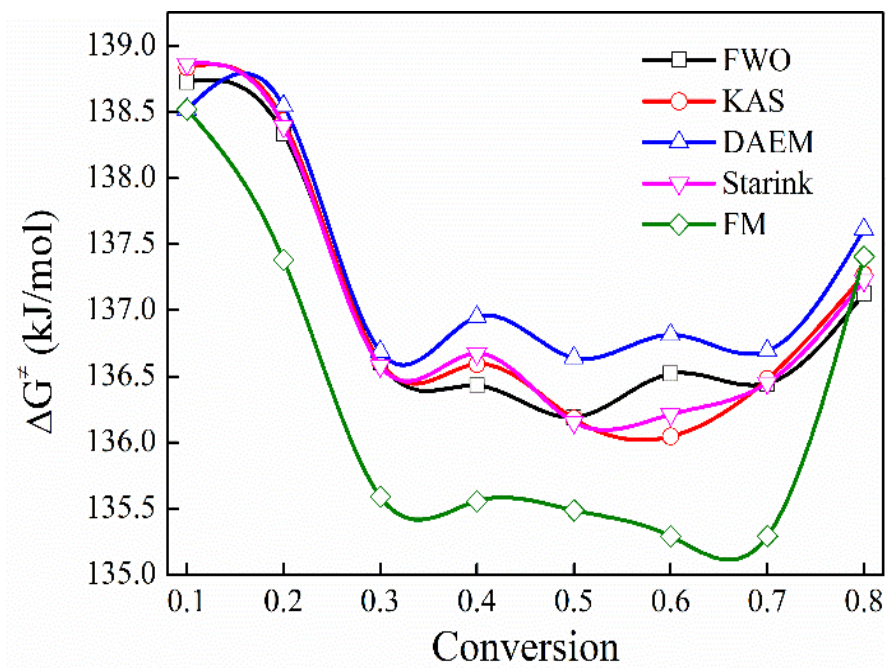
(e)

Fig. 5. Kinetic and thermodynamic parameters with respect to conversion value. (a) average apparent activation energy (E_a); (b) average Pre-exponential factor (A); (c) average enthalpy of reaction ($\Delta H^{\neq}$); (d) average Gibbs free energy ($\Delta G^{\neq}$); (e) average entropy change ($\Delta S^{\neq}$).

Click here to access/download

Supplementary Interactive Plot Data (CSV)

Supplementary material-2020.12.30.docx
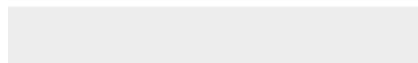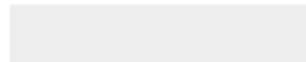
Credit Author Statement

Jinjia Du: Conceptualization, Investigation, Writing-original draft. **Lei Gao**: Conceptualization, Investigation, Writing-original draft. **Yong Yang**: Writing-review & editing. **Guo Chen**: Writing-review & editing. **Shenghui Guo**: Supervision, Project administration, Writing-review & editing. **Mamdouh Omran**: Writing review & editing. **Jin Chen**: Funding acquisition, Writing-review & editing. **Roger Ruan**: Writing review & editing.

Declaration of interests

☒ The authors declare that they have no known competing financial interests or personal relationships that could have appeared to influence the work reported in this paper.

☐The authors declare the following financial interests/personal relationships which may be considered as potential competing interests: